# POLITECNICO DI TORINO
# Repository ISTITUZIONALE

Facile preparation of antifouling nanofiltration membrane by grafting zwitterions for reuse of shale gas wastewater

*Publisher copyright*

(Article begins on next page)

21 December 2022

# Facile preparation of antifouling nanofiltration membrane by grafting zwitterions for reuse of shale gas wastewater

Minli Hu [a,b], Qidong Wu [a,b], Chen Chen [c], Songmiao Liang [d], Yuanhui Liu [a,b], Yuhua Bai [e],

Alberto Tiraferri [f], Baicang Liu [a,b,*]

[a] Key Laboratory of Deep Earth Science and Engineering (Ministry of Education), College of Architecture and Environment, Institute of New Energy and Low-Carbon Technology, Institute for Disaster Management and Reconstruction, Sichuan University, Chengdu, Sichuan 610207, PR China

[b] Yibin Institute of Industrial Technology, Sichuan University Yibin Park, Section 2, Lingang Ave, Cuiping District, Yibin, Sichuan 644000, PR China

[c] Litree Purifying Technology Co., Ltd, Haikou, Hainan 571126, PR China

[d] Vontron Technology Co., Ltd, Guiyang 550018, PR China

[e] Infrastructure Construction Department, Chengdu University, Chengdu 610106, PR China

[f] Department of Environment, Land and Infrastructure Engineering, Politecnico di Torino, Corso Duca degli Abruzzi 24, 10129 Turin, Italy

**Abstract:** Complex organic matter causes severe fouling when membranes are applied for shale gas wastewater (SGW) treatment. This study reports the grafting of a zwitterionic polymer brush consisting of poly (sulfobetaine methacrylate) (PSBMA) onto the surface of a commercial nanofiltration (NF) membrane via electron transfer-atom transfer radical polymerization (ARGET-ATRP) to achieve anti-fouling property, especially against organic foulants. Compared to the pristine NF membranes, the PSBMA-grafted NF membrane showed high performance when challenged by SGW as a feed stream: (1) The productivity was significantly improved during long-term operation, with a 64.28% increase in flux at 50% recovery rate of SGW, while maintaining a near constant ion removal rate; (2) According to fluorescence regional integration under the Excitation—Emission—Matrix Spectra, the removal of protein-like organic matters and humus-like organic matters increased by 34.01% and 16.48%, respectively; (3) The XDLVO theory demonstrated that the hydrophobic interactions between the membrane surface and organic foulants were reduced by increasing the Lewis acid-base interaction energy. The proposed anti-fouling zwitterionic membranes has potential in industrial application for the on-site reuse of SGW.

## 1. Introduction

The "shale gas revolution" was first successfully practiced in the USA to ensure energy security. China is currently accelerating the pace of shale gas exploration and development [1, 2]. According to evaluations made by the Chinese government, China has $25.08 \times 10^{12}$ m$^3$ of technically recoverable shale gas reserves, positioning it as one of the most promising countries in the world for shale gas development [3, 4]. However, the shale gas exploration process consumes large amounts of freshwater resources and generates vast quantities of shale gas wastewater (SGW) [5, 6]. In the Sichuan Basin, China, the average freshwater demand of a shale gas well is 23,650–34,000 m$^3$, and 8-70% of the shale gas flowback and produced water is returned to the ground [7-9].

SGW in the Sichuan Basin contains low to moderate salinity (total dissolved solids < 30 g/L), complex and heterogeneous organic compounds, and its treatment to safe standard is costly and challenging [10]. Currently, most SGW both in China and USA are reused for fracturing in new wells, since the recycling of the fracturing fluid can achieve both cost savings and environmental pollution reduction [11-13]. The effective removal of divalent ions is critical for SGW reuse to avoid scaling on production equipment and in the shale formation [14-16]. Based on the salinity and composition of the Sichuan Basin SGW, nanofiltration (NF) membrane technology is a suitable and promising candidate for purification with the aim to remove divalent ions and maintain a stable production of shale gas [9, 17, 18]. However, membrane fouling is a major drawback that restricts the application of NF membranes and can lead to increased energy consumption, alongside increased frequency of chemical cleaning and shortened membrane life [19-21]. In general, membrane fouling is the result of a complex series of physicochemical interactions between the membrane surface and the fouling agents [21, 22][23, 24]. The complex organic mixture in SGW is arguably the main cause of NF membrane fouling in this application [25]. Effective pretreatments are often used

60  to improve the NF performance and ensure its sustainable operation [13, 26]. The

61  combination of coagulation [27], adsorption [28], ozone pre-oxidation [29], or biological

62  treatment technology [30] with UF has been applied for pre-treatment. However, NF fouling

63  is still inevitable and few studies have focused on the properties of the NF membrane itself to

64  improve their resistance to contamination from SGW foulants.

65  The synthesis of new antifouling membranes through surface modification is an effective

66  way to control membrane fouling [22], and direct modification of the membrane surface is

67  ideal for large-scale processing applications [31-33]. Antifouling membrane modification

68  materials are mainly polymers, and the introduction of hydrophilic monomers or polar groups

69  can significantly improve the membrane antifouling performance [34, 35]. Commonly used

70  modifiers include: poly(vinyl alcohol) (PVA) [36], polyethylene glycol (PEG) [37], MXene

71  [38], polydopamine (PDA) [39], and polyurethane[40]. Compared to other hydrophilic

72  materials, zwitterionic polymer brushes (e.g., sulfobetaine methacrylate, SBMA) comprising

73  both anionic and cationic end groups exhibit excellent antifouling performance at high salt

74  concentrations [41], because of their overall electrical neutrality and strong hydration ability.

75  SBMA can form a tight hydration layer on the surface of membrane materials, which can

76  weaken the interaction force between organic pollutants and the membrane surface [21, 31,

77  41-48]. In particular, this mechanism is effective against hydrophobic organic substances,

78  such as protein-like and humic-like matter, which accounts for a relatively high proportion of

79  the organics in SGW [28, 29, 35, 49]. Typical modification methods include chemical

80  grafting, physical coating, and polymer modification [44, 45, 47]. Modification through

81  activators regenerated by electron transfer–atom transfer radical polymerization (ARGET-

82  ATRP) is suitable to modify the membrane surface at large scale under routine industrial

83  conditions in an easy and quick way, because it only require a low dosage of copper catalyst

84  and has high tolerance to oxygen presence [50, 51]. Our previous study used ARGET-ATRP

85  method to graft [2-(methacryloyloxy) ethyl] dimethyl(3-sulfopropyl) ammonium hydroxide

86  (DMAPS) on the surface of self-made green ultrafiltration membranes showing highly

87  promising results also for other membrane processes and applications [52].

88      In this work, we tune and apply this procedure to fabricate a high-performance NF

89  membrane deployed to treat SGW with the goal of reuse. The relationship between membrane

90  surface modification and improved antifouling performance is investigated upon grafting a

91  zwitterionic polymer brush PSBMA onto the surface of a commercial NF membranes via an

92  ARGET-ATRP method. The water flux decline rate is analyzed and evaluated in the light of

93  the membrane surface properties and the degree of organic deposition. The effect of

94  membrane fouling is discussed using the XDLVO theory. The purpose of this paper is to

95  provide valuable information on ways to reduce NF membrane fouling by designing NF

96  membranes suitable for shale gas wastewater treatment.

97

98  **2. Materials and methods**

99  2.1. Pretreatment of the raw water

100  The raw water in this study was acquired from one of the reservoirs of the Weiyuan shale

101  gas play, Sichuan, China. The detailed water quality and the optimal pretreatment conditions

102  were comprehensively analyzed in our previous study [13]. In brief, the optimal pretreatment

103  condition for coagulation involved addition of 900 mg/L ferric chloride hexahydrate

104  ($FeCl_3 \cdot 6H_2O$) followed by 30 min settling. The supernatant was then introduced to the tank of

105  a ultrafiltration system comprising a submerged hollow fiber poly (vinylidene fluoride)

106  (PVDF) UF membrane (Litree Purifying Technology Co., Ltd. Haikou, China with nominal

107  molecular weight cut-off 100 kDa under a constant flux of 50 L $m^{-2}h^{-1}$).

108  2.2. Materials

109     Two types of commercially available NF membranes were employed in this work, namely,

110     the membranes referred to as VNF1 (Vontron Membrane Technology Co., Ltd., Guiyang,

111     China), and NF90 (DuPont, USA). Ultrapure water was supplied by a Ulupure ultrapure water

112     purification system (Chengdu, China) with a resistivity of 18.25 MΩ. Sulfobetaine

113     methacrylate (SBMA), sometimes referred to as 3-dimethyl (methacryloyloxyethyl)

114     ammonium propane sulfonate (DMAPS), N,N-dimethylformamide (DMF)，l-ascorbic acid,

115     copper (II) chloride, tris (2-pyridylmethyl) amine (TPMA), magnesium sulfate ($MgSO_4$,

116     anhydrous, reagent plus, ≥99.5%), and sodium chloride (NaCl, reagent grade, 99%) were

117     obtained from Sigma Aldrich (USA), Dopamine hydrochloride, α-bromoisobutyryl bromide

118     (BiBB, 98%), isopropyl alcohol (IPA), tris (hydroxymethyl) aminomethane (Tris) (>99.8%),

119     and triethylamine (TEA) (>99%), were purchased from Aladdin (China). Sodium sulfate

120     ($Na_2SO_4$) (anhydrous, ≥99%), magnesium chloride ($MgCl_2$) (≥98%), and ethylene glycol

121     (99%) were all analytical reagents (Kelong Chemical, Chengdu, China). Glycerol (99.7%)

122     was purchased from VWR (PA, USA). Diiodomethane (99%) was purchased from Macklin

123     (Shanghai, China).

124     2.3 Surface modification of NF membranes

125     The commercial membrane was subject to surface ARGET-ATRP grafting reaction

126     through a typical three-step strategy. The first step involved the preparation of a BiBB-

127     initiator-dopamine solution; after addition of the Tris buffer into this solution to adjust the pH,

128     the commercial membrane was placed into the buffered solution to form a PDA surface

129     coating (seond step); the third step encompassed the grafting of SBMA to the membrane

130     surface through the ARGET-ATRP reaction. The detailed steps can be found in **Text S1 (SI)**.

131

132
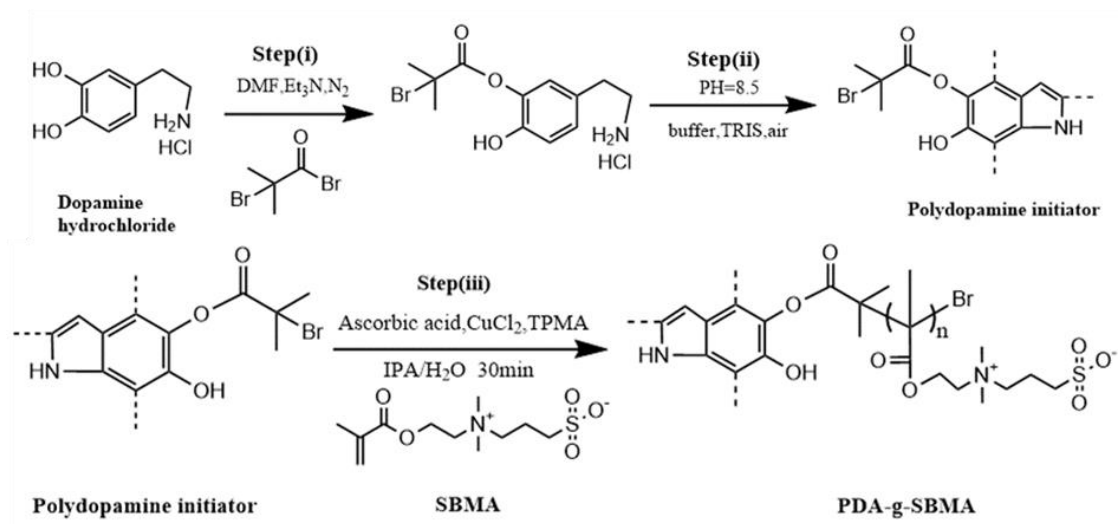
**Scheme. 1.** Proposed modification of NF membranes and reaction products: Step (i) involved the reaction of dopamine hydrochloride and 2-bromoisobutyryl bromide; Step (ii) in which the reaction mixture from Step (i) was added to Tris buffer (pH=8.5) to form a BiBB-initiator-PDA coating; Step (iii) involved the surface initiated ARGET-ATRP reaction with SBMA from the BiBB-initiator-PDA coating to produce modified membranes with a surface-grafted SBMA polymer brush.

2.4. Membrane Characterization

The surface chemical composition of the membranes was analyzed via X-ray photoelectron spectroscopy (XPS) (Axis Supra, Kratos Analytical Ltd., UK) and with a Fourier transform infrared (FTIR) spectrometer equipped with a diamond attenuated total reflection (ATR) attachment (Nicolet is iS20, Thermo Fisher Scientific Inc., USA). The membrane surface morphology and roughness characteristics were obtained by scanning electron microscopy (SEM) (Regulus 8230, Hitachi, Japan) and atomic force microscopy (AFM, Dimension Icon, Bruker, Germany), respectively. The zeta potential was evaluated by a SurPASS™ 3 electrokinetic analyzer (Anton Paar, Austria). The dynamic water contact angles were determined by a contact angle measurement equipment (KRÜSS GmbH, Germany) at room temperature. More details can be found in our previous study [53] and in **Text S2 (SI)**.

151    2.5 Separation performance of the NF membranes

152    The NF lab unit was thoroughly cleaned before and after each fouling experiment. Prior to

153    each experiment, the membranes were soaked in ultrapure water at room temperature for 24 h

154    and then compacted with ultrapure water at a pressure of 6.89 bar (100 psi) for at least 30 min.

155    The separation performance of the membranes was evaluated at an applied pressure of 20.7

156    bar (300 psi) in a stainless-steel dead-end membrane module (HP 4750, Sterlitech Corp., Kent,

157    WA), with an effective testing area, A, of 14.6 cm$^2$. The separation equipment was operated

158    under constant stirring of 300 rpm to minimize concentration polarization effects. Eq. (1) was

159    employed to determine the flux of pure water:

160    $$J = \frac{V}{A \times \Delta t} \qquad (1)$$

161    where V (L) is calculated by dividing the permeate water mass collected in a certain

162    interval ($\Delta t$) by the water density.

163    The ion filtration performance of the NF membranes was evaluated using inorganic salts

164    ($Na_2SO_4$, $MgSO_4$, $MgCl_2$, $NaCl$) in water with a concentration of 2000 mg/L. The salt solute

165    rejection (R) was obtained at steady-state by Eq (2).

166    $$R = 1 - \frac{C_p}{(C_0 + C_f)/2} \qquad (2)$$

167    where $C_P$ and $C_0$ represent the concentration of the solute in the permeate and that in the

168    feed, respectively, while $C_f$ is the concentration of the solute in the final concentrated feed.

169    Electric conductivity measured by calibrated ultrameter II 6PFC conductivity meter (Myron L

170    Company) was used as a proxy for salt concentration. The presented rejection values for each

171    sample are the average of three different measurements collected over a 60 min period.

172    2.6 Anti-fouling properties

173    The normalized permeate flux in the fouling stage was calculated using Eq. (3) [54][59]:

8

174 $$normalized\ flux = \frac{J}{J_0} \qquad (3)$$

175 where J is the permeate flux at any given time during the test, and $J_0$ is the initial permeate

176 flux. The slope of the plot of $J/J_0$ versus recovery rate (%, v/v) yielded the fouling propensity

177 of the NF membranes [54].

178 To determine the surface tension characteristics of a solid surface, two of the three probe

179 liquids should be polar and the other should be non-polar, and the test reagents must have

180 high surface tension parameters [55]. In this study, the surface of the pristine NF membranes

181 and the modified NF membranes are regarded as solid. The two polar liquids were ultrapure

182 water and glycerol, while the non-polar liquid was diiodomethane. The surface tension

183 properties of each probe liquid are listed in **Table S1 (SI)**. The surface tension parameters of

184 the materials were calculated by measuring the direct contact angle of the three probe liquids

185 and using a modified form of the extended Young equation given by:

186 $$\gamma_L^{TOT} = \gamma_L^{LW} + \gamma_L^{AB} \qquad (4)$$

187 $$\gamma_L^{AB} = 2\sqrt{\gamma_L^+ \gamma_L^-} \qquad (5)$$

188 $$(1+\cos\theta)\gamma_L = 2(\sqrt{\gamma_S^{LW}\gamma_L^{LW}} + \sqrt{\gamma_S^+\gamma_L^-} + \sqrt{\gamma_S^-\gamma_L^+}) \qquad (6)$$

189 According to the 'extended DLVO' or 'XDLVO' theory, in the water environment, the

190 interfacial energy between membranes and foulants is the sum of the Lifshitz–van der Waals

191 (LW), electrostatic double layer (EL), and Lewis acid–base (AB) interactions. The

192 electrostatic force (EL) interaction energy ( $\Delta G_{mlf}^{EL}$ ) is also one component of the total

193 interaction free energy, but it is much smaller than $\Delta G_{mlf}^{TOT}$, and can thus be neglected,

194 resulting in:

195 $$\Delta G_{mlf}^{TOT} = \Delta G_{mlf}^{LW} + \Delta G_{mlf}^{AB} \qquad (7)$$

196    $$\Delta G_{mlf}^{LW} = -2(\sqrt{\gamma_f^{LW}} - \sqrt{\gamma_l^{LW}})(\sqrt{\gamma_m^{LW}} - \sqrt{\gamma_l^{LW}}) \tag{8}$$

197    $$\Delta G_{mlf}^{AB} = 2[\sqrt{\gamma_l^+}(\sqrt{\gamma_m^-} + \sqrt{\gamma_f^-} - \sqrt{\gamma_l^-}) + \sqrt{\gamma_l^-}(\sqrt{\gamma_m^+} + \sqrt{\gamma_f^+} - \sqrt{\gamma_l^+}) - (\sqrt{\gamma_m^+\gamma_f^-} + \sqrt{\gamma_m^-\gamma_f^+})] \tag{9}$$

198    The subscripts f, l, and m represent the foulant, the liquid medium, and the membrane

199    surface, respectively. Statistical analysis was performed with the statistical software SPSS

200    18.0.

201    **3. Results and discussion**

202    3.1 Membrane surface properties

203    Membrane surface characteristics, such as chemical structure, hydrophilicity, roughness,

204    and charge determine the separation performance and the anti-fouling properties of the

205    membrane [42, 56]. **Fig. 1(A)** presents that the ATR-FTIR spectra determined between 500

206    $cm^{-1}$ and 4000 $cm^{-1}$ for the pristine NF90 and VNF1 membranes, the BiBB-initiation-PDA

207    mobilized membranes (NF90-PDA, VNF1-PDA), and the PDA-g-PSBMA modified NF

208    membranes (NF90-PSBMA, VNF1-PSBMA). The stretching vibration peak at 1578, 1504,

209    1487 $cm^{-1}$ is attributed to the superposition of the peak of the polyamide layer and the

210    polysulfone layer in the benzene ring plane. The characteristic peaks of the polysulfone

211    support layer can be observed: specifically, the symmetric stretching vibration peaks of

212    O=S=O at 1167 and 1149 $cm^{-1}$, and the asymmetric stretching vibration peaks of O=S=O at

213    1320 and 1296 $cm^{-1}$. VNF1 series membranes are significantly different from NF90 series

214    membranes in that only the latter showed peaks at 1610 $cm^{-1}$ (H-bonded C=O stretching) and

215    1540 $cm^{-1}$ (N–H in-plane bending and C–N bending vibration stretching vibration of the

216    group –CO–NH-, amide II band) [57, 58]. Therefore, the characteristic peaks of amide II and

217    arylamide were not observed for the VNF1 series membranes, suggesting that the latter

218    consist of piperazine amide. The common peak between the two membranes at 1664 $cm^{-1}$ is

219    attributed to the amide I band (C=O and C-N stretching vibration, C-C-N deformation

220    vibration) [59, 60]. After the grafting of the PSBMA brushes, new peaks at 1715 and 1038

221     cm$^{-1}$ emerged, attributed to ester and sulfonate groups of SBMA, respectively. These results

222     preliminarily indicate that PSBMA was successfully grafted on the NF membrane surfaces

223     [48, 61].
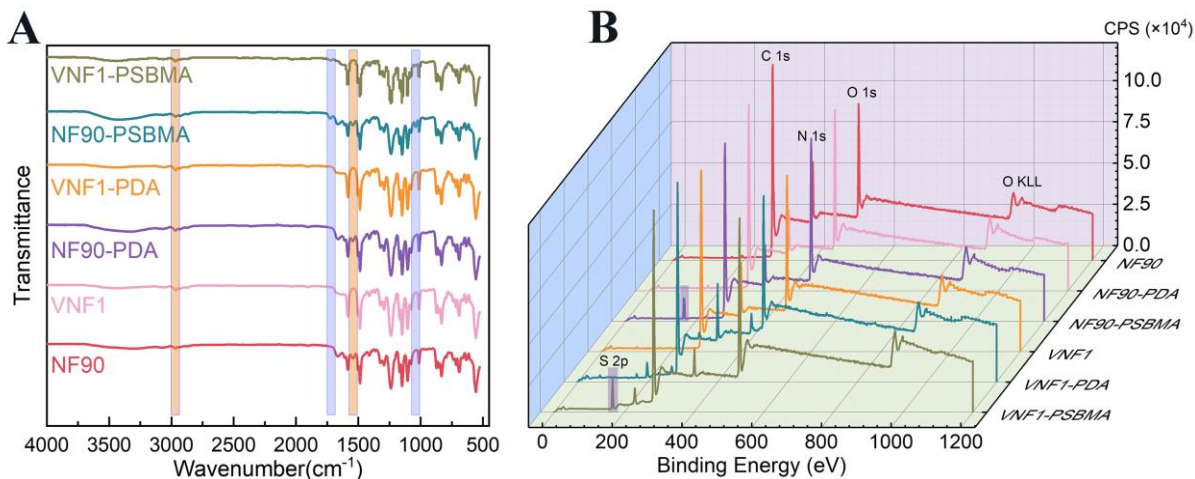


225     **Fig. 1. (A)** ATR-FTIR spectra and **(B)** XPS spectra of pristine NF90 and VNF1 membranes

226     and modified membranes prepared from PDA immobilization and PSBMA grafting.

227

228     To further analyze the chemical composition of the NF90/VNF1 membrane surfaces

229     before and after modification, XPS analysis was conducted and the resulting surface

230     elemental compositions and spectra are presented in **Table 1** and **Fig. 1(B)**, respectively. An

231     obvious increase in the O atom content and a decrease in N atom content were clearly

232     observed upon PBSMA grafting. Consequently, the O/C atomic ratios of NF90-PSBMA and

233     VNF1-PSBMA were respectively higher than those of NF90 and VNF1, while the N/C atomic

234     ratios were lower. This result is rationalized with the fact that the grafted PSBMA has high

235     O/C atomic ratio and low O/N atomic ratio compared with the pure polyamide. These results

236     further confirm that PSBMA was successfully introduced onto the NF membrane surfaces.

237

238     **Table 1** Surface elemental composition of the membranes.

| Membrane No. | Atomic percent (%) | | Atomic ratio |
|---|---|---|---|

| | C | N | O | Br | O/N | O/C |
|---|---|---|---|---|---|---|
| NF90 | 74.29 | 10.56 | 15.15 | 0 | 1.43 | 0.20 |
| NF90-PDA | 72.86 | 7.63 | 19.47 | 0.04 | 2.55 | 0.27 |
| NF90-PSBMA | 72.33 | 7.33 | 20.31 | 0.03 | 2.77 | 0.28 |
| VNF1 | 74.52 | 8.54 | 16.81 | 0 | 1.97 | 0.23 |
| VNF1-PDA | 75.04 | 8.14 | 16.76 | 0.13 | 2.06 | 0.22 |
| VNF1-PDA | 73.64 | 4.62 | 21.67 | 0.07 | 4.69 | 0.29 |

239

240 3.2. Morphology analysis and surface charge

241 The morphology and roughness of the membrane surface influence the membrane

242 hydrophilicity, water flux, and the interactions between the surface and foulants. The surface

243 morphology of the NF90 and VNF1 membranes did not change significantly upon

244 modification with PSBMA (**Fig. 2**). According to the AFM results, the root means square

245 roughness parameters (Rq) of the NF90, NF90-PDA, and NF90-PSBMA membrane were

246 54.4±2.1 nm, 38.7±3.7 nm, and 29.0±0.6 nm, respectively, while those of VNF1, VNF1-PDA,

247 and VNF1-PSBMA membrane were 5.04±0.1 nm, 4.68±0.2 nm, and 3.87±0.7 nm,

248 respectively. Therefore, the roughness of the membrane surfaces decreased by approximately

249 20% after coating with PDA and by approximately 45% upon modification with the

250 zwitterion, with respect to the pristine membranes (**Fig. 3A**). This result suggest that the

251 modification steps may level out the surface features of polyamide. However, the initial

252 roughness of the two membranes was already small and the observed reduction was not

253 substantial in absolute terms, thus likely not resulting in significant changes in membrane

254 performance during operation.

255
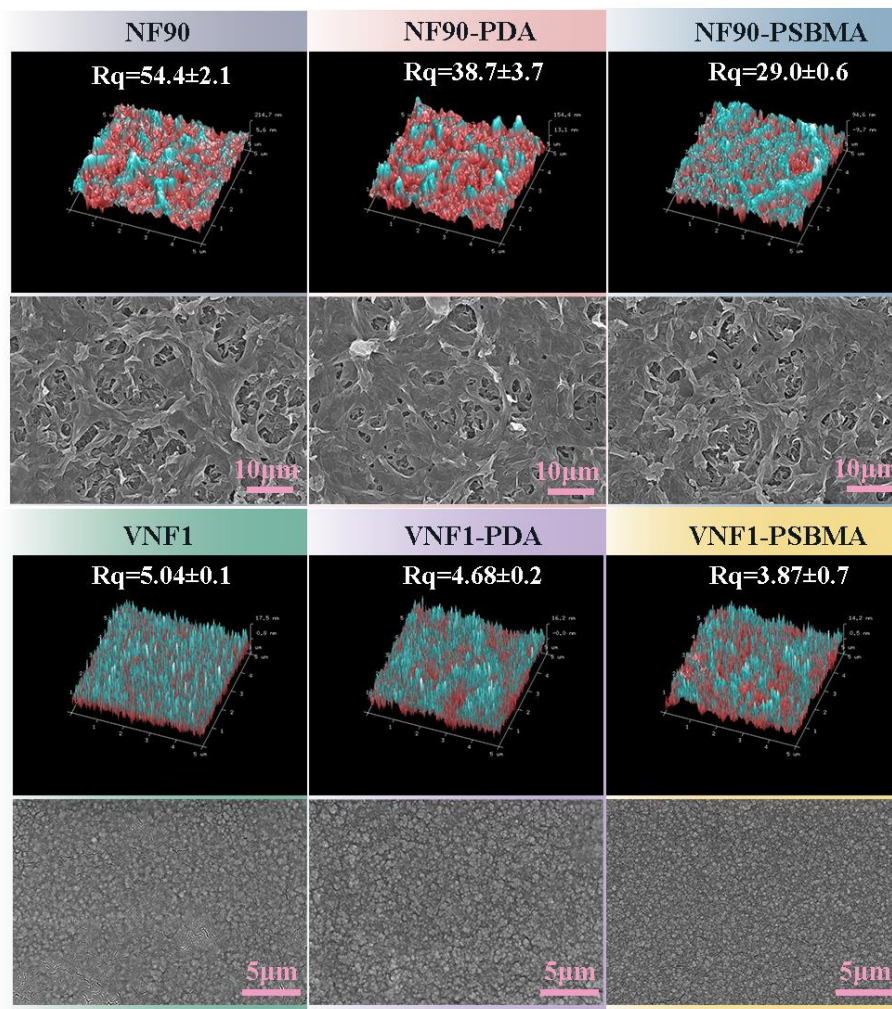
**Fig. 2.** AFM and SEM images of pristine NF90 and VNF1 membranes and modified membranes prepared by immobilizing PDA and by grafting PSBMA.

258



259
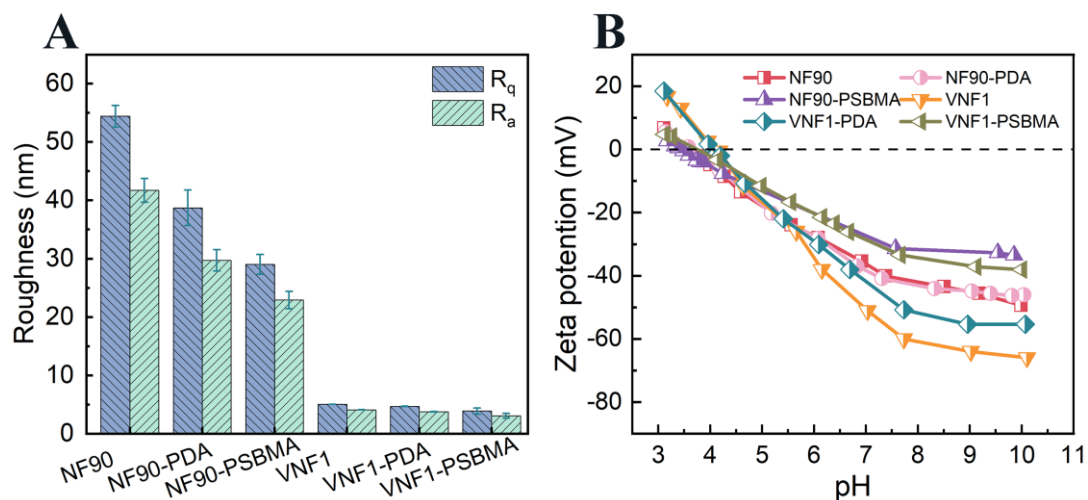
**Fig. 3. (A)** The average values of root mean-square (Rq) and average roughness (Ra) were calculated from AFM images using at least six different locations on each membrane sample (NF90, NF90-PDA, NF90-PSBMA, VNF1, VNF1-PDA and VNF1-PSBMA); **(B)** Surface zeta potential values of pristine NF90 and VNF1 membrane and modified membranes as a function of pH.

The surface properties of the modified membranes were further investigated by acquiring zeta potential values. As shown in **Fig. 3B**, the pristine NF90 and VNF1 membranes had highly negative electric potential, due to the carboxyl groups typically resulting from interfacial polymerization of polyamide. With the coating of PDA, the amine and hydroxyl groups of dopamine generally reduced the magnitude of the negative potential, which was then further reduced upon SBMA grafting due to the net zero charge properties of the zwitterions [62]. This trend was more pronounced in the VNF1 membrane samples, for which a potential of larger magnitude was measured at the surface of the pristine membrane. However, the zeta potential curves of the membranes modified with the PSBMA brush layer was practically thre same, regardless of the starting material, suggesting that the modification was successful in both cases.

The wettability of the membrane surface was evaluated through water contact angle measurements **(Fig. 4A)**. The initial contact angles of pristine NF90 membrane, NF90-PDA membrane, and NF90-PSBMA membrane were 55.2±0.9°, 48.7±1.5°, and 46.0±2.3°, respectively, while the initial contact angles of pristine VNF1 membrane, VNF1-PDA membrane, and VNF1-PSBMA membrane were 52.5±1.9°, 41.6±2.65°, and 28.4±0.99°, respectively. The presence of PDA increased the wettability, although this enhancement effect was minor, owing to the short reaction time (10 min). On the other hand, the water contact

angle decreased significantly after growth of the zwitterionic polymers brush, especially for

the VNF1 samples.
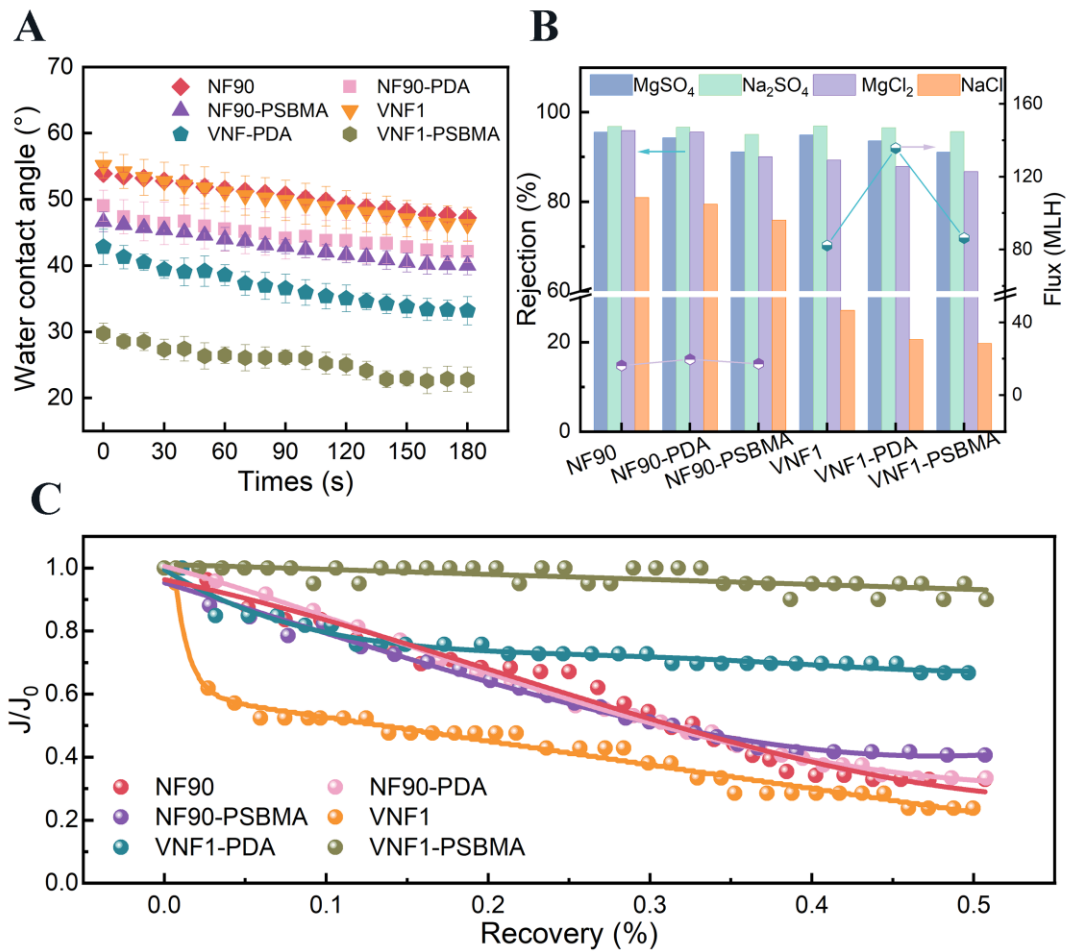


**Fig. 4. (A)** Water contact angle variation in time of pristine NF90 and VNF1 membranes and

modified membranes; **(B)** Salt rejection values of pristine NF90 and VNF1 membrane and

modified membranes (2.068 MPa, 25 °C, salt concentration: 2000 mg/L); **(C)** Permeate flux

as a function of tecovery rate for the different membranes (operating pressure: 2.068MPa;

maximum water recovery: 50%).

Considering the selectivity shown in **Fig. 4B**, all the membranes had much higher rejection

to divalent ions than monovalent ions, exhibiting a typical NF performance. In general, the

observed rejection was in the order $Na_2SO_4$ > $MgSO_4$ > $MgCl_2$ > NaCl. With the coating of

dopamine and the grafting of PSBMA, the retention rate of all the ions was slightly reduced,

but overall, there was no significant loss of the original retention rate. During filtration of ultrapure water, the average flux were 16.2, 19.7, and 17.3 LMH for NF90, NF90-PDA and NF90-PSBMA, while the permeate flux of VNF1-based samples were much higher, with average fluxes equal to 82.2, 135.6, and 86.3 LMH for VNF1, VNF1-PDA and VNF1-PSBMA, respectively. Compared to the VNF1 membranes, the NF90 membranes are denser and therefore provide higher retention of monovalent ions and correspondingly lower fluxes. In both cases, the flux increased significantly following PDA coating and returned to lower values upon zwitterion brush formation. Ultimately, the values observed for the zwitterion-grafted membranes were slightly higher than those measured for pristine membranes.

**Fig. 4C** illustrates the fouling behavior (revealing itself as a decrease in permeate flux [63]) of the membranes during the dead-end NF process for feed streams coinciding with the effluents of integrated coagulation-UF pre-treatment. Grafting of SBMA greatly improved the resistance to foulant deposition and to flux reduction. While the water flux was reduced compared to the membranes with only PDA attached, the performance of the membranes modified with PSBMA brushes was maintained for a longer period of time. The effect of VNF1 modification was significantly better than that of NF90, consistent with the results of FTIR and previous literature reports [13], likely due to the different chemistry of the polyamide constituting the two membranes. The flux measured by deploying the VNF1-PSBMA membrane was nearly constant during the filtration test, indicating negligible or inconsequential deposition of foulants on these samples.

It is usually difficult to draw an overall profile of organic pollutants in shale gas wastewaters and their process variations. Three-dimensional excitation-emission matrix (EEM) fluorescence spectroscopy was used to analyze fluorescent organics compositions in a complicated system such as the SWG of this study, by simultaneously varying the excitation and emission wavelengths in real time (**Fig. 5**) [64]. As detailed in our previous study [29],

322 the fluorescence regional integration (FRI) method allowed classification of the organic

323 compounds in five domains: region I (Ex/Em = 220–250/280–330 nm, aromatic protein),

324 region II (Ex/Em = 220–250/330–380 nm, aromatic protein), region III (Ex/Em = 220–

325 250/380–480 nm, fulvic acid-like matters), region IV (Ex/Em = 250–440/280–380 nm,

326 soluble microbial by-product-like matters), and region V (Ex/Em = 250–400/380–540 nm,

327 humic acid-like components). According to the FRI under the EEM corresponding to each

328 region volume, almost no removal of dissolved organic matter was achieved after coagulation,

329 while the hybrid UF process mainly remove fulvic acid-like components, humic acid-like

330 components, and phenolic compounds (**Fig 6B**). The fraction of dissolved organics removed

331 by NF90 membrane was 94.1% for region III, 93.5% for region V, 87.7% for region II, 74.6%

332 for region IV, and 37.9% for region I. Larger removal rates were observed for the modified

333 NF90-PSBMA membranes, but in the same order: III (96.3%), V (95.4%), II (91.2%), IV

334 (88.7%), I (83.7%). The same order of removal rate was also determined for VNF1 samples,

335 with a higher rate relative to the modified membrane with respect to the pristine one.

336 Specifically, while the removal rate of dissolved organics by VNF1 was III (85.8%), V

337 (84.2%), II (78.6%), IV (51.1%), I (8.2%), that provided by VNF1-PSBMA was III (93.7%),

338 V (91.7%), II (90.5%), IV (85.5%), I (80.3%). These results and those presented in **Fig. 5**

339 clearly shows that the modified membranes improved the removal rate of organic matter in

340 each of the areas, but more markedly that of protein-like organic matter, which may be due to

341 the combination of increased membrane density and hydrophilicity following the surface

342 modification.
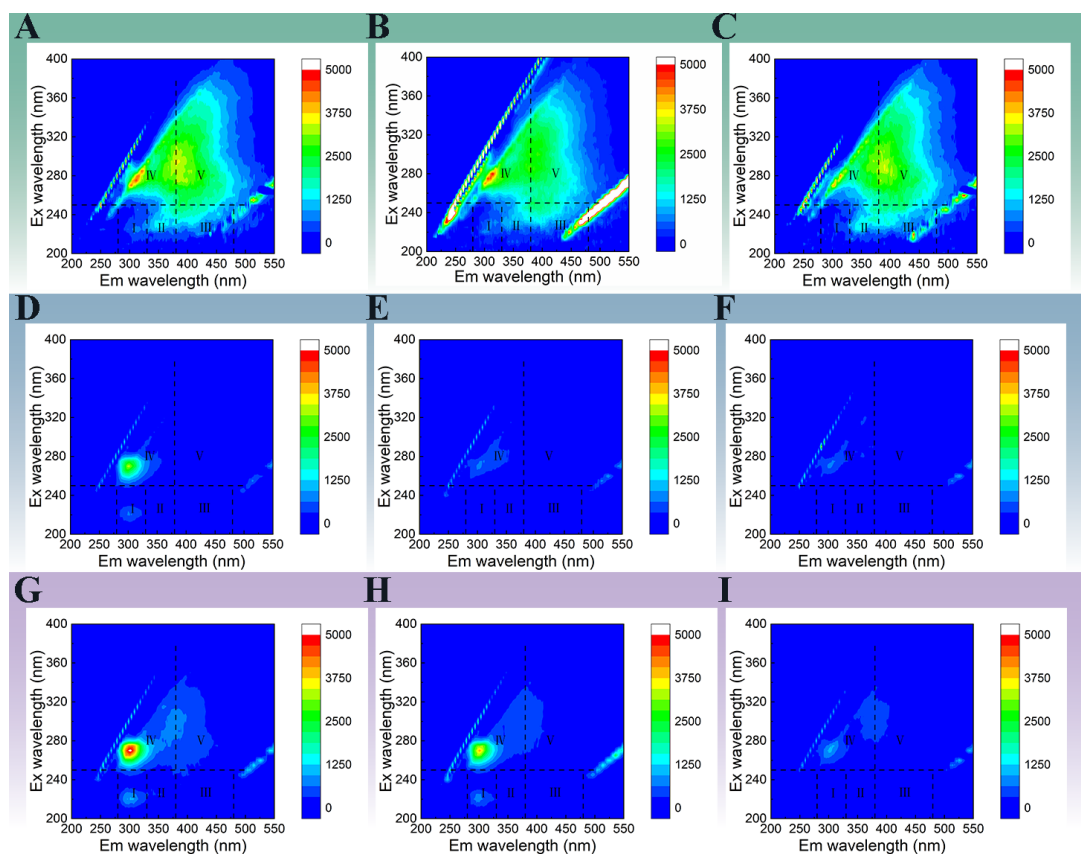
**Fig. 5.** Fluorescence excitation-emission matrix (EEM) of effluent water from each treatment process: (A) Raw water; (B) Coagulation; (C) Ultrafiltration; filtration through (D) NF90, (E) NF90-PDA, (F) NF90-PSBMA (G) VNF1, (H) VNF1-PDA, or (I) VNF1-PSBMA membranes. (I: tyrosine protein-like substances, II: tryptophan protein-like substances, III: fulvic-like substances, IV: soluble microbial byproducts, V: humic-like substances.)

3.4. Membrane-foulant physicochemical interactions

Extended XDLVO calculations are an accepted method to account for the interfacial forces between two surfaces at the microscopic scale [65]. In this paper, this theory was applied to investigate the main forces acting between the NF membranes and the SGW colloids. The contact angles of water, glycerol, and diiodomethane on the membrane surface and when in contact with a layer of SGW colloids are summarized in **Table S2 (SI)**. The resulting surface energy components ($\gamma^{LW}$, $\gamma^+$, $\gamma^-$) were calculated using **eqs. 4-6**, and the

18

357 results are shown in **Table 2**. $\Delta G_{mlf}^{LW}$ and $\Delta G_{mlf}^{AB}$ were thus obtained with **eqs. 8** and **9**,

358 respectively, and the results are also presented in **Table 2**. Following surface grafting of the

359 zwitterionic polymers SBMA, the electron acceptor component ($\gamma^+$) slightly increased, while

360 the electron donor component ($\gamma^-$) increased importantly. This phenomenon is rationalized

361 mainly with the fact that the -SO$_3$ group of SBMA is negatively charged in water, and can

362 enhance the electron donating capability, hence the hydrophilicity of the membrane surface

363 [52]. Repulsion forces thwart the adsorption of contaminants on the membrane surface: the

364 more positive is the interaction energy, the more it is repulsive, and the membrane surface is

365 less likely to be fouled [66, 67]. Both AB and LW components of the membranes-SGW

366 colloids interaction had positive sign, thus the total interaction free energy ($\Delta G_{mlf}^{TOT}$) had

367 positive sign for all the membrane samples. Significantly, the surface grafting of SBMA

368 provided much more positive values of the total interfacial free energy, implying that the

369 zwitterionic SBMA brushes effectively reduced the likelihood of foulant adhesion on the

370 membrane surfaces. Furthermore, we found that the Lewis acid-base interaction energy

371 ($\Delta G_{mlf}^{AB}$) was much higher than the Lifshitzvan der Waals interaction energy ($\Delta G_{mlf}^{LW}$) and that

372 $\Delta G_{mlf}^{LW}$ remained almost unchanged after surface grafting, while $\Delta G_{mlf}^{AB}$ increased significantly.

373 Therefore, the Lewis acid-base interaction energy ($\Delta G_{mlf}^{AB}$) played the key role in controlling

374 membrane fouling.
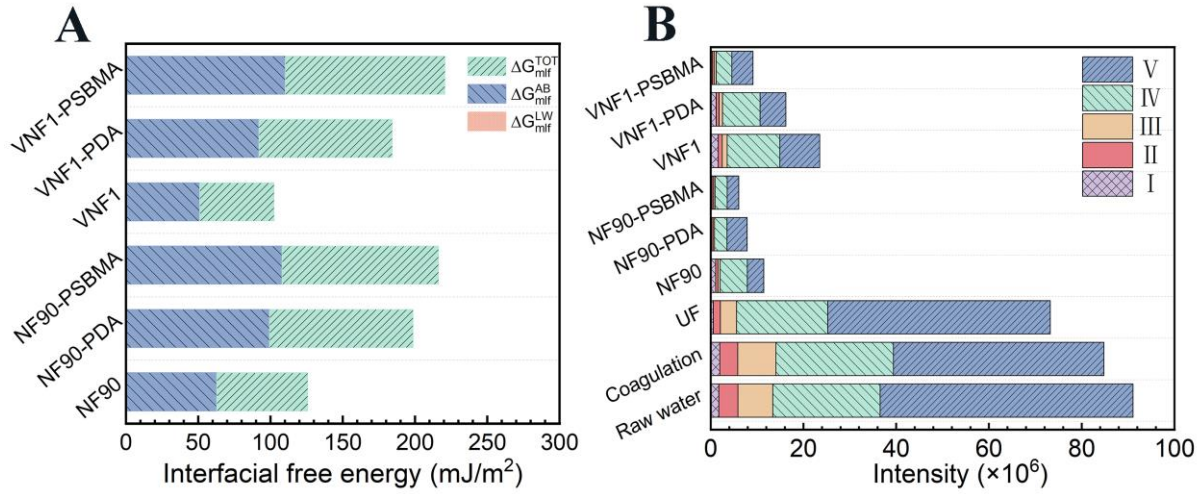
**Fig. 6. (A)** Total interaction energy ($\Delta G_{mlf}^{TOT}$), Lifshitz–van der Waals interaction energy ($\Delta G_{mlf}^{LW}$), and Lewis acid–base (AB) interaction energy ($\Delta G_{mlf}^{AB}$) between the membranes and the SGW particles in aqueous solution; **(B)** Fluorescence region integral (FRI) results for samples from the effluent of each treatment process.

**Table 2**

The surface tension parameters and interfacial free energy of all membranes and SGW particles (mJ/m$^2$).

| Item | Surface tension parameter (mJ/m$^2$) | | | | | Free Energy | | |
|---|---|---|---|---|---|---|---|---|
| | $\gamma_L^{LW}$ | $\gamma_L^-$ | $\gamma_L^+$ | $\gamma_L^{AB}$ | $\gamma_L^{TOT}$ | $\Delta G^{LW}$ | $\Delta G^{AB}$ | $\Delta G^{TOT}$ |
| NF90 | 33.956 | 21.135 | 0.156 | 3.626 | 37.582 | 0.516 | 62.341 | 62.857 |
| NF90-PDA | 33.388 | 42.664 | 0.004 | 0.797 | 34.185 | 0.494 | 98.839 | 99.333 |
| NF90-PSBMA | 30.249 | 49.483 | 0.002 | 0.568 | 30.818 | 0.370 | 107.746 | 108.116 |
| VNF1 | 33.608 | 20.041 | 2.224 | 13.354 | 46.961 | 0.502 | 50.695 | 51.198 |
| VNF1-PDA | 33.759 | 37.450 | 0.005 | 0.899 | 34.659 | 0.508 | 91.573 | 92.081 |
| VNF1- | 30.456 | 53.440 | 0.113 | 4.921 | 35.377 | 0.378 | 109.957 | 110.336 |

PSBMA

384

## Conclusion

386    Zwitterionic SBMA brushes were grafted onto the surface of commercial NF membranes,

387    greatly improving the membrane antifouling ability and organic removal while retaining high

388    values of water permeability and only slightly decreasing the rejection rate of conventional

389    monovalent and divalent ions. The VNF1-PSBMA membrane exhibited very high

390    performance with pure water flux of 86.3 LMH, sodium sulfate removal rate of 95.67%, and

391    with the $J/J_0$ ratio upon fouling 73.54% higher than that related to the pristine VNF1

392    membrane at 50% recovery of SGW. All the dissolved organics were removed effectively by

393    the VNF1-PSBMA membrane, but especially the protein-like organic matter, which was not

394    rejected effectively by the pristine membranes. Antifouling and organic removal experiments

395    showed that the modification of membranes with grafted zwitterionic has high potential to

396    control membrane fouling and improve membrane performance in SGW reuse. This work

397    proposes a membrane modification that effectively affords better membrane performance,

398    particularly for the treatment of a highly complex wastewater from the shale gas industry,

399    thus providing a successful exploration of modified membrane materials and industrial

400    applications.

401

409    **References**

410    [1] C. Jia, M. Zheng, Y. Zhang, Unconventional hydrocarbon resources in China and the
411    prospect of exploration and development, Petroleum Exploration and Development, 39 (2012)
412    139-146.
413    [2] H. Chang, T. Li, B. Liu, R.D. Vidic, M. Elimelech, J.C. Crittenden, Potential and
414    implemented membrane-based technologies for the treatment and reuse of flowback and
415    produced water from shale gas and oil plays: A review, Desalination, 455 (2019) 34-57.
416    [3] C.L. Weber, C. Clavin, Life Cycle Carbon Footprint of Shale Gas: Review of Evidence
417    and Implications, Environ. Sci. Technol., 46 (2012) 5688-5695.
418    [4] S. Jiang, J. Zhang, Z. Jiang, Z. Xu, D. Cai, L. Chen, Y. Wu, D. Zhou, Z. Jiang, X. Zhao, S.
419    Bao, Geology, resource potentials, and properties of emerging and potential China shale gas
420    and shale oil plays, Interpretation, 3 (2015) SJ1-SJ13.
421    [5] C.T. Montgomery, M.B. Smith, Hydraulic fracturing: History of an enduring technology,
422    JPT, Journal of Petroleum Technology, 62 (2010) 26-32.
423    [6] R. Beckwith, Hydraulic fracturing: The fuss, the facts, the future, JPT, Journal of
424    Petroleum Technology, 62 (2010) 34-41.
425    [7] Jackson, B. Robert, Vengosh, Avner, Davies, J. Richard, Carey, J. William, O'Sullivan,
426    Francis, The Environmental Costs and Benefits of Fracking, Annual review of environment
427    and resources, (2014).
428    [8] A. Kondash, A. Vengosh, Water Footprint of Hydraulic Fracturing, Environmental
429    Science & Technology Letters, 2 (2015) 276-280.
430    [9] N.A. Ahmad, P.S. Goh, L.T. Yogarathinam, A.K. Zulhairun, A.F. Ismail, Current
431    advances in membrane technologies for produced water desalination, Desalination, 493
432    (2020).
433    [10] B.C. Gordalla, U. Ewers, F.H. Frimmel, Hydraulic fracturing: a toxicological threat for
434    groundwater and drinking-water?, Environmental Earth Sciences, 70 (2013) 3875-3893.
435    [11] W. Shang, A. Tiraferri, Q. He, N. Li, H. Chang, C. Liu, B. Liu, Reuse of shale gas
436    flowback and produced water: Effects of coagulation and adsorption on ultrafiltration, reverse
437    osmosis combined process, Sci. Total Environ., 689 (2019) 47-56.
438    [12] P. Tang, J. Li, T. Li, L. Tian, Y. Sun, W. Xie, Q. He, H. Chang, A. Tiraferri, B. Liu,
439    Efficient integrated module of gravity driven membrane filtration, solar aeration and GAC
440    adsorption for pretreatment of shale gas wastewater, J. Hazard. Mater., (2020).
441    [13] H. Chang, B. Liu, B. Yang, X. Yang, C. Guo, Q. He, S. Liang, S. Chen, P. Yang, An
442    integrated coagulation-ultrafiltration-nanofiltration process for internal reuse of shale gas
443    flowback and produced water, Sep. Purif. Technol., 211 (2019) 310-321.
444    [14] K.B. Gregory, R.D. Vidic, D.A. Dzombak, Water Management Challenges Associated
445    with the Production of Shale Gas by Hydraulic Fracturing, Elements, 7 (2011) 181-186.
446    [15] T. Tong, K.H. Carlson, C.A. Robbins, Z. Zhang, X. Du, Membrane-based treatment of
447    shale oil and gas wastewater: The current state of knowledge, Frontiers of Environmental
448    Science and Engineering, 13 (2019).
449    [16] B. Wang, M. Xiong, P. Wang, B. Shi, Chemical characterization in hydraulic fracturing
450    flowback and produced water (HF-FPW) of shale gas in Sichuan of China, Environmental
451    Science and Pollution Research, 27 (2020) 26532-26542.
452    [17] F.X. Kong, Z.P. Wang, Z. Ji, J.F. Chen, C.M. Guo, G.D. Sun, Y.F. Xie, Organic fouling
453    of membrane distillation for shale gas fracturing flowback water desalination: A special
454    interest in the feed properties by pretreatment, Environmental Science: Water Research and
455    Technology, 5 (2019) 1339-1348.

456 [18] D. Liu, J. Li, C. Zou, H. Cui, Y. Ni, J. Liu, W. Wu, L. Zhang, R. Coyte, A. Kondash, A.
457 Vengosh, Recycling flowback water for hydraulic fracturing in Sichuan Basin, China:
458 Implications for gas production, water footprint, and water quality of regenerated flowback
459 water, Fuel, 272 (2020) 117621.
460 [19] A.W. Mohammad, Y.H. Teow, W.L. Ang, Y.T. Chung, D.L. Oatley-Radcliffe, N. Hilal,
461 Nanofiltration membranes review: Recent advances and future prospects, Desalination, 356
462 (2015) 226-254.
463 [20] D. Zhou, L. Zhu, Y. Fu, M. Zhu, L. Xue, Development of lower cost seawater
464 desalination processes using nanofiltration technologies — A review, Desalination, 376
465 (2015) 109-116.
466 [21] D. Rana, T. Matsuura, Surface Modifications for Antifouling Membranes, Chem. Rev.,
467 110 (2010) 2448-2471.
468 [22] X. Zhao, R. Zhang, Y. Liu, M. He, Y. Su, C. Gao, Z. Jiang, Antifouling membrane
469 surface construction: Chemistry plays a critical role, J. Membr. Sci., 551 (2018) 145-171.
470 [23] S. Jiang, Y. Li, B.P. Ladewig, A review of reverse osmosis membrane fouling and
471 control strategies, Sci. Total Environ., 595 (2017) 567-583.
472 [24] T. Nguyen, F.A. Roddick, L. Fan, Biofouling of water treatment membranes: a review of
473 the underlying causes, monitoring techniques and control measures, Membranes (Basel), 2
474 (2012) 804-840.
475 [25] E. Mohammad-Pajooh, D. Weichgrebe, G. Cuff, B.M. Tosarkani, K.-H. Rosenwinkel,
476 On-site treatment of flowback and produced water from shale gas hydraulic fracturing: A
477 review and economic evaluation, Chemosphere, 212 (2018) 898-914.
478 [26] W. Yu, T. Liu, J. Crawshaw, T. Liu, N. Graham, Ultrafiltration and nanofiltration
479 membrane fouling by natural organic matter: Mechanisms and mitigation by pre-ozonation
480 and pH, Water Res., 139 (2018) 353-362.
481 [27] F.-x. Kong, J.-f. Chen, H.-m. Wang, X.-n. Liu, X.-m. Wang, X. Wen, C.-m. Chen, Y.F.
482 Xie, Application of coagulation-UF hybrid process for shale gas fracturing flowback water
483 recycling: Performance and fouling analysis, J. Membr. Sci., 524 (2017) 460-469.
484 [28] Y. Liu, P. Tang, Y. Zhu, W. Xie, P. Yang, Z. Zhang, B. Liu, Green aerogel adsorbent for
485 removal of organic compounds in shale gas wastewater: High-performance tuning and
486 adsorption mechanism, Chem. Eng. J., 416 (2021) 129100.
487 [29] P. Tang, B. Liu, Y. Zhang, H. Chang, P. Zhou, M. Feng, V.K. Sharma, Sustainable reuse
488 of shale gas wastewater by pre-ozonation with ultrafiltration-reverse osmosis, Chem. Eng. J.,
489 392 (2020) 123743.
490 [30] P. Tang, W. Xie, A. Tiraferri, Y. Zhang, J. Zhu, J. Li, D. Lin, J.C. Crittenden, B. Liu,
491 Organics removal from shale gas wastewater by pre-oxidation combined with biologically
492 active filtration, Water Res., 196 (2021) 117041.
493 [31] Y.-C. Chiang, Y. Chang, C.-J. Chuang, R.-C. Ruaan, A facile zwitterionization in the
494 interfacial modification of low bio-fouling nanofiltration membranes, J. Membr. Sci., 389
495 (2012) 76-82.
496 [32] T. Sun, Y. Liu, L. Shen, Y. Xu, R. Li, L. Huang, H. Lin, Magnetic field assisted
497 arrangement of photocatalytic TiO2 particles on membrane surface to enhance membrane
498 antifouling performance for water treatment, J. Colloid Interface Sci., 570 (2020) 273-285.
499 [33] M. He, K. Gao, L. Zhou, Z. Jiao, M. Wu, J. Cao, X. You, Z. Cai, Y. Su, Z. Jiang,
500 Zwitterionic materials for antifouling membrane surface construction, Acta Biomater., 40
501 (2016) 142-152.
502 [34] Z. Wang, D. Hou, S. Lin, Composite Membrane with Underwater-Oleophobic Surface
503 for Anti-Oil-Fouling Membrane Distillation, Environ. Sci. Technol., 50 (2016) 3866-3874.

504  [35] F.-x. Kong, G.-d. Sun, J.-f. Chen, J.-d. Han, C.-m. Guo, Z. Tong, X.-f. Lin, Y.F. Xie,
505  Desalination and fouling of NF/low pressure RO membrane for shale gas fracturing flowback
506  water treatment, Sep. Purif. Technol., 195 (2018) 216-223.
507  [36] X. Chen, T. Taguchi, Enhanced Skin Adhesive Property of Hydrophobically Modified
508  Poly(vinyl alcohol) Films, ACS Omega, 5 (2020) 1519-1527.
509  [37] D.T. Auguste, R.K. Prud'homme, P.L. Ahl, P. Meers, J. Kohn, Polymer-Protected
510  Liposomes: Association of Hydrophobically-Modified PEG with Liposomes, in: Polymeric
511  Drug Delivery I, American Chemical Society, 2006, pp. 95-120.
512  [38] H. Huang, Y. Sun, L. Cui, Y. Ni, S. Li, W. Xing, W. Jing, Generation of Monodisperse
513  Submicron Water-in-Diesel Emulsions via a Hydrophobic MXene-Modified Ceramic
514  Membrane, Ind. Eng. Chem. Res., 59 (2020) 20349-20358.
515  [39] C. Zhao, X. Yu, X. Da, M. Qiu, X. Chen, Y. Fan, Fabrication of a charged
516  PDA/PEI/Al2O3 composite nanofiltration membrane for desalination at high temperatures,
517  Sep. Purif. Technol., 263 (2021) 118388.
518  [40] P. Kanagaraj, I.M.A. Mohamed, W. Huang, C. Liu, Membrane fouling mitigation for
519  enhanced water flux and high separation of humic acid and copper ion using hydrophilic
520  polyurethane modified cellulose acetate ultrafiltration membranes, Reactive and Functional
521  Polymers, 150 (2020) 104538.
522  [41] H. Liu, Z. Ma, W. Yang, X. Pei, F. Zhou, Facile preparation of structured zwitterionic
523  polymer substrate via sub-surface initiated atom transfer radical polymerization and its
524  synergistic marine antifouling investigation, Eur. Polym. J., 112 (2019) 146-152.
525  [42] Q. Li, X. Zhang, H. Yu, H. Zhang, J. Wang, A facile surface modification strategy for
526  improving the separation, antifouling and antimicrobial performances of the reverse osmosis
527  membrane by hydrophilic and Schiff-base functionalizations, Colloids and Surfaces A:
528  Physicochemical and Engineering Aspects, 587 (2020) 124326.
529  [43] C. Liu, A.F. Faria, J. Ma, M. Elimelech, Mitigation of Biofilm Development on Thin-
530  Film Composite Membranes Functionalized with Zwitterionic Polymers and Silver
531  Nanoparticles, Environ. Sci. Technol., 51 (2017) 182-191.
532  [44] M.S. Rahaman, H. Therien-Aubin, M. Ben-Sasson, C.K. Ober, M. Nielsen, M.
533  Elimelech, Control of biofouling on reverse osmosis polyamide membranes modified with
534  biocidal nanoparticles and antifouling polymer brushes, J Mater Chem B, 2 (2014) 1724-
535  1732.
536  [45] D. Saeki, T. Tanimoto, H. Matsuyama, Anti-biofouling of polyamide reverse osmosis
537  membranes using phosphorylcholine polymer grafted by surface-initiated atom transfer
538  radical polymerization, Desalination, 350 (2014) 21-27.
539  [46] J. Wang, Z. Wang, J. Wang, S. Wang, Improving the water flux and bio-fouling
540  resistance of reverse osmosis (RO) membrane through surface modification by zwitterionic
541  polymer, J. Membr. Sci., 493 (2015) 188-199.
542  [47] G. Ye, J. Lee, F. Perreault, M. Elimelech, Controlled Architecture of Dual-Functional
543  Block Copolymer Brushes on Thin-Film Composite Membranes for Integrated "Defending"
544  and "Attacking" Strategies against Biofouling, ACS Appl. Mater. Interfaces, 7 (2015) 23069-
545  23079.
546  [48] W.-W. Yue, H.-J. Li, T. Xiang, H. Qin, S.-D. Sun, C.-S. Zhao, Grafting of zwitterion
547  from polysulfone membrane via surface-initiated ATRP with enhanced antifouling property
548  and biocompatibility, J. Membr. Sci., 446 (2013) 79-91.
549  [49] H. Chang, T. Li, B. Liu, C. Chen, Q. He, J.C. Crittenden, Smart ultrafiltration membrane
550  fouling control as desalination pretreatment of shale gas fracturing wastewater: The effects of
551  backwash water, Environ. Int., 130 (2019) 104869.
552  [50] K. Matyjaszewski, Atom Transfer Radical Polymerization (ATRP): Current status and
553  future perspectives, Macromolecules, 45 (2012) 4015-4039.

554    [51] K. Matyjaszewski, D. Hongchen, W. Jakubowski, J. Pietrasik, A. Kusumo, Grafting from
555    surfaces for "everyone": ARGET ATRP in the presence of air, Langmuir, 23 (2007) 4528-
556    4531.
557    [52] W. Xie, A. Tiraferri, X. Ji, C. Chen, Y. Bai, J.C. Crittenden, B. Liu, Green and
558    sustainable method of manufacturing anti-fouling zwitterionic polymers-modified poly(vinyl
559    chloride) ultrafiltration membranes, J. Colloid Interface Sci., 591 (2021) 343-351.
560    [53] M. He, T. Li, M. Hu, C. Chen, B. Liu, J. Crittenden, L.-Y. Chu, H.Y. Ng, Performance
561    improvement for thin-film composite nanofiltration membranes prepared on PSf/PSf-g-PEG
562    blended substrates, Sep. Purif. Technol., 230 (2020) 115855.
563    [54] S. Hong, M. Elimelech, Chemical and physical aspects of natural organic matter (NOM)
564    fouling of nanofiltration membranes, J. Membr. Sci., 132 (1997) 159-181.
565    [55] W. Wu, R.F. Giese, C.J. van Oss, Stability versus flocculation of particle suspensions in
566    water—correlation with the extended DLVO approach for aqueous systems, compared with
567    classical DLVO theory, Colloids and Surfaces B: Biointerfaces, 14 (1999) 47-55.
568    [56] A. Tiraferri, Y. Kang, E.P. Giannelis, M. Elimelech, Highly Hydrophilic Thin-Film
569    Composite Forward Osmosis Membranes Functionalized with Surface-Tailored
570    Nanoparticles, ACS Appl. Mater. Interfaces, 4 (2012) 5044-5053.
571    [57] C.Y. Tang, Y.-N. Kwon, J.O. Leckie, Effect of membrane chemistry and coating layer on
572    physiochemical properties of thin film composite polyamide RO and NF membranes: II.
573    Membrane physiochemical properties and their dependence on polyamide and coating layers,
574    Desalination, 242 (2009) 168-182.
575    [58] A. Simon, W.E. Price, L.D. Nghiem, Influence of formulated chemical cleaning reagents
576    on the surface properties and separation efficiency of nanofiltrationmembranes, J. Membr.
577    Sci., 432 (2013) 73-82.
578    [59] M.F. Jimenez Solomon, Y. Bhole, A.G. Livingston, High flux membranes for organic
579    solvent nanofiltration (OSN)—Interfacial polymerization with solvent activation, J. Membr.
580    Sci., 423-424 (2012) 371-382.
581    [60] Y. Li, E. Wong, Z. Mai, B. Van der Bruggen, Fabrication of composite
582    polyamide/Kevlar aramid nanofiber nanofiltration membranes with high permselectivity in
583    water desalination, J. Membr. Sci., 592 (2019).
584    [61] M.R. De Guzman, C.K.A. Andra, M.B.M.Y. Ang, G.V.C. Dizon, A.R. Caparanga, S.-H.
585    Huang, K.-R. Lee, Increased performance and antifouling of mixed-matrix membranes of
586    cellulose acetate with hydrophilic nanoparticles of polydopamine-sulfobetaine methacrylate
587    for oil-water separation, J. Membr. Sci., 620 (2021) 118881.
588    [62] Q. Shi, Y. Su, W. Zhao, C. Li, Y. Hu, Z. Jiang, S. Zhu, Zwitterionic Polyethersulfone
589    Ultrafiltration Membrane with Superior Antifouling Property, J. Membr. Sci., 319 (2008) 271.
590    [63] Z. He, D.J. Miller, S. Kasemset, D.R. Paul, B.D. Freeman, The effect of permeate flux on
591    membrane fouling during microfiltration of oily water, J. Membr. Sci., 525 (2017) 25-34.
592    [64] J. Guo, X. Zhu, Q. Wang, W. Liu, Y. Wang, The combination effect of preozonation and
593    CNTs layer modification on low-pressure membrane fouling control in treating NOM and
594    EfOM, J. Membr. Sci., 627 (2021) 119225.
595    [65] M. Zhang, X. Zhou, L. Shen, X. Cai, F. Wang, J. Chen, H. Lin, R. Li, X. Wu, B.-Q. Liao,
596    Quantitative evaluation of the interfacial interactions between a randomly rough sludge floc
597    and membrane surface in a membrane bioreactor based on fractal geometry, Bioresour.
598    Technol., 234 (2017) 198-207.
599    [66] C. Liu, D. Song, W. Zhang, Q. He, X. Huangfu, S. Sun, Z. Sun, W. Cheng, J. Ma,
600    Constructing zwitterionic polymer brush layer to enhance gravity-driven membrane
601    performance by governing biofilm formation, Water Res., 168 (2020) 115181.

602    [67] N. Subhi, A.R.D. Verliefde, V. Chen, P. Le-Clech, Assessment of physicochemical
603    interactions in hollow fibre ultrafiltration membrane by contact angle analysis, J. Membr.
604    Sci., 403-404 (2012) 32-40.

605    **Graphical abstract**

606